

Geophysical Research Letters

RESEARCH LETTER

10.1029/2018GL081110

Key Points:

- Arctic sea ice loss affects the Hadley cell only through ocean-atmosphere coupling
- Arctic sea ice loss acts as a negative internal feedback in the response of the Hadley cell width to anthropogenic emissions
- Ocean heat transport opposes the thermodynamic effect of Arctic sea ice loss on the Hadley circulation

Correspondence to:

R. Chemke,
rc3101@columbia.edu

Citation:

Chemke, R., Polvani, L. M., & Deser, C. (2019). The effect of Arctic sea ice loss on the Hadley circulation. *Geophysical Research Letters*, *46*, 963–972. <https://doi.org/10.1029/2018GL081110>




Received 26 OCT 2018

Accepted 12 JAN 2019

Accepted article online 16 JAN 2019

Published online 29 JAN 2019

The Effect of Arctic Sea Ice Loss on the Hadley Circulation

R. Chemke¹ , L. M. Polvani^{1,2} , and C. Deser³ 

¹Department of Applied Physics and Applied Mathematics, Columbia University, New York, NY, USA, ²Department of Earth and Environmental Sciences and Lamont-Doherty Earth Observatory, Columbia University, Palisades, NY, USA, ³National Center for Atmospheric Research, Boulder, CO, USA

Abstract One of the most robust responses of the climate system to future greenhouse gas emissions is the melting of Arctic sea ice. It is thus essential to elucidate its impacts on other components of the climate system. Here we focus on the response of the annual mean Hadley cell (HC) to Arctic sea ice loss using a hierarchy of model configurations: atmosphere only, atmosphere coupled to a slab ocean, and atmosphere coupled to a full-physics ocean. In response to Arctic sea ice loss, as projected by the end of the 21st century, the HC shows negligible changes in the absence of ocean-atmosphere coupling. In contrast, by warming the Northern Hemisphere thermodynamic coupling weakens the HC and expands it northward. However, dynamic coupling acts to cool the Northern Hemisphere which cancels most of this weakening and narrows the HC, thus opposing its projected expansion in response to increasing greenhouse gases.

Plain Language Summary The climate's response to anthropogenic emissions comprises different feedbacks of the different components in the climate system. One of the robust responses to increased greenhouse gases is the melting of Arctic sea ice, which is found to have large effects on the hydrological circulation in the atmosphere. Here we examine the effect of Arctic sea ice loss on the tropical circulation. We find that under Arctic sea ice loss ocean heat transport acts to transfer the Arctic signal to the tropics and to contract the tropical circulation. This contraction opposes the projected widening of the tropical circulation and thus shows that Arctic sea ice loss acts as a negative internal feedback in the response of the tropical circulation to increased greenhouse gases.

1. Introduction

The melting of Arctic sea ice in recent decades is one of the prominent instances of climate change. Over the last decades, perennial Arctic sea ice has decreased its extent by 25–35% and with unabated emissions of greenhouse gases is projected to nearly vanish by the end of the 21st century (Intergovernmental Panel on Climate Change, 2013). In spite of the substantial loss of Arctic sea ice in recent decades, its effects on the atmospheric circulation remain unclear, mostly due to numerous confounding processes in the climate system, the short period of the observed record, and the large internal climate variability (e.g., Barnes, 2013; Barnes & Polvani, 2015; Blackport & Kushner, 2016; Cohen et al., 2014; Hassanzadeh & Kuang, 2015; Overland et al., 2015; Screen & Simmonds, 2013; Sun et al., 2016; Vihma, 2014; Walsh, 2014).

At midlatitudes, the projected effects of Arctic sea ice loss on the zonal wind are found to oppose the effects by increased greenhouse gases. In response to Arctic sea ice loss, the Northern Hemisphere (NH) jet weakens on its poleward flank, in concert with the reduced meridional temperature gradient accompanying polar amplification (e.g., Deser et al., 2015, 2016; Oudar et al., 2017; Peings & Magnusdottir, 2014; Screen et al., 2018; Smith et al., 2017; Sun et al., 2015). Concomitantly, tropospheric eddy momentum fluxes are also projected to weaken (in agreement with a reduction in baroclinicity; Oudar et al., 2017). The projected effects of Arctic sea ice loss on the position of the jet (its meandering), however, are less certain (e.g., Barnes & Polvani, 2015; Barnes & Screen, 2015; Hassanzadeh & Kuang, 2015; Oudar et al., 2017; Screen & Simmonds, 2013). And, in the tropics the Intertropical Convergence Zone (ITCZ) shifts equatorward and intensifies in response to the projected Arctic sea ice loss (e.g., Deser et al., 2015; Smith et al., 2017; Tomas et al., 2016; Wang et al., 2018).

Interestingly, ocean-atmosphere coupling is found to play an important role in the above circulation changes. Thermodynamic coupling (i.e., changes in sea surface temperature, SST, by radiative and turbulent

heat fluxes) is found to warm the NH, mostly at high latitudes, and thus to reduce the meridional temperature gradient, to weaken the mean zonal wind on its poleward flank, and to push the ITCZ northward (similarly, cooling the NH was found to shift the ITCZ southward due to thermodynamic coupling; Chiang & Bitz, 2005; Kang et al., 2008). In contrast, dynamic coupling (i.e., the effects of ocean heat transport on the SST) was found to cool the NH, by transferring heat to the Southern Hemisphere (SH), strengthen the jet on its equatorward flank, shift it equatorward, and to push the ITCZ equatorward (e.g., Deser et al., 2015, 2016; Green & Marshall, 2017; Tomas et al., 2016; Wang et al., 2018). One example of a change in ocean circulation under Arctic sea ice loss is the weakening of the Atlantic meridional overturning circulation (e.g., S'avellec et al., 2017), which may then affect the tropical circulation (e.g., Zhang & Delworth, 2005).

The main focus in all the above studies is the impact of Arctic sea ice loss on the ITCZ and the extratropical circulation. The aim of this work, however, is to investigate the effects of the projected Arctic sea ice loss on the Hadley cell (HC). While there is an extensive literature on the HC response to projected anthropogenic emissions (e.g., Held & Soden, 2006; Kang et al., 2013; Lu et al., 2007; Merlis, 2015; Vallis et al., 2015), the specific impact of Arctic sea ice loss is largely unexplored. By the end of this century, climate projections show a weakening of the HC along with an expansion of its vertical and meridional extents (Intergovernmental Panel on Climate Change, 2013; Kang et al., 2013; Vallis et al., 2015). Recently, Tomas et al. (2016) and Wang et al. (2018) showed that in response to Arctic sea ice loss thermodynamic coupling also acts to weaken the NH HC, while ocean dynamics acts to strengthen it, thus opposing its projected weakening. Building on the work of Tomas et al. (2016) and Wang et al. (2018), here we examine not only the HC strength but also its northward edge and vertical extent and ask what fraction of the HC response to anthropogenic forcing is caused by the melting of Arctic sea ice. In addition, we here elucidate the physical mechanisms behind the HC response to Arctic sea ice loss. Since the circulation response to Arctic sea ice loss is more prominent in the NH, we focus here on the NH HC response.

2. Methods

To study the response of the annual mean HC to Arctic sea ice loss, we make use of the set of simulations presented in Deser et al. (2016). These simulations were conducted using the Community Climate System Model version 4 (CCSM4; Gent et al., 2011), where all components (atmosphere, ocean, land, and ice) have $\sim 1^\circ$ horizontal resolution.

Since ocean-atmosphere coupling plays an important role in transferring the Arctic sea ice signal to lower latitudes, three configurations of the CCSM4 are used: (i) atmosphere only, with prescribed SST and sea ice and no active ocean model (NOM), (ii) slab ocean model (SOM), which lacks any changes in ocean heat transport but accounts for ocean-atmosphere thermodynamic coupling, and (iii) full-depth ocean model (FOM), which accounts for both ocean-atmosphere thermodynamic and dynamic coupling.

The approach taken here for achieving a desired Arctic sea ice state is to add a spatially and seasonally varying longwave radiative flux (LRF) to the ice component in the SOM and FOM (see Deser et al., 2015 for details). Two experiments were conducted: one where the LRF is designed to reproduce the Arctic sea ice thickness and concentration of the end of the 20th century (1980–1999) and one of the end of the 21st century (2080–2099), based on model simulations forced with the historical and RCP8.5 scenarios, respectively. Note that since only the Arctic sea ice is different between the two experiments (i.e., radiative forcing is fixed at year 2000), and the LRF is added solely to the ice component, with no heat conduction between the ice and ocean components, any changes in the atmosphere and ocean stem from changes in Arctic sea ice alone. For the NOM, the sea ice in both experiments is prescribed based on its corresponding FOM simulation. For the NOM 21st century the SST in regions of Arctic sea ice loss is prescribed based on the FOM 21st century; elsewhere the SST is prescribed based on the FOM twentieth century in both experiments. This accounts for the local ocean warming due to sea ice loss (Deser et al., 2015; Screen & Simmonds, 2013; Screen et al., 2015). This procedure introduces discontinuities in SST at the edge of the region where sea ice is projected to disappear; however, these discontinuities are much smaller than those already present across the ocean-ice boundary in the twentieth century. The results shown below for the NOM, SOM, and FOM are computed using the last 260 years of a 260-, 300-, and 360-year run, respectively. Throughout the paper, Δ represents the difference between the end of the 21st and 20th centuries Arctic sea ice simulations.

Finally, in order to assess the importance of Arctic sea ice loss in affecting the HC, Δ FOM is compared to the response of the HC to the full anthropogenic forcing (RCP8.5). The latter is computed by averaging the

six available CCSM4 runs of the historical and RCP8.5 scenarios at the end of the 20th (1980–1999) and 21st centuries (2080–2099), respectively. This mean of all six runs isolates the forced response of the HC by averaging out the internal variability.

Note that since the SST and sea ice in the NOM configuration are prescribed, the difference between Δ SOM and Δ NOM isolates the effects of ocean-atmosphere thermodynamic coupling. In addition, since an identical Q-flux and mixed-layer depth are used for the two LRF experiments in the SOM configuration, the difference between Δ FOM and Δ SOM isolates the effects of ocean-atmosphere dynamic coupling.

To characterize the HC, following Chemke and Polvani (2018), the width, strength and height of the annual mean HC are calculated as follows:

(i) The northern edge of the HC ($\phi_{\Psi_{500}}$) is calculated at 500 mb as the latitude where the meridional mass stream function (Ψ),

$$\Psi(\phi, p) = \frac{2\pi a \cos \phi}{g} \int_0^p \bar{v}(\phi, p) dp', \quad (1)$$

first changes sign northward of its maximum value, where p is pressure, v is meridional velocity, over-bar represents zonal and time mean, g is gravity, and a is Earth's radius.

(ii) The strength of the HC (Ψ_{\max}) is calculated as the maximum value of Ψ at 500 mb in the NH.

(iii) The height of the HC (H) is calculated as the tropopause height averaged over 10° latitude centered around Ψ_{\max} . The tropopause height is estimated as the lowest level where the temperature lapse rate reaches 2 K/km.

Throughout the paper all tropical quantities are averaged between the latitude of the ITCZ (defined as the latitude where Ψ switches sign between the southern and northern HC's branches) and $\phi_{\Psi_{500}}$, and all subtropical quantities between 30° N and 40° N.

3. Results

We start by comparing the temperature and circulation responses to sea ice melting in the NOM, SOM, and FOM configurations (Figure 1). For the sake of clarity, here we present the results for all model configurations and their differences in a single figure. While a few of these results have appeared in Deser et al. (2016), Tomas et al. (2016), and Wang et al. (2018), aggregating these results allows us to make a clear comparison, as was done for the extratropical NH circulation in Deser et al. (2016). As shown in Deser et al. (2016), since the prescribed SST in the NOM 21st century is based on the FOM 21st century simulation only in regions where Arctic sea ice loss occurs, the warming of the SST in Δ NOM is confined to the Arctic (Figure 1a). And, similar to Tomas et al. (2016), allowing thermodynamic ocean-atmosphere coupling, Δ SOM shows warming of both hemispheres but mostly at NH high latitudes (Figure 1b). This effect of the thermodynamic coupling can also be seen by plotting the difference in SST response between Δ SOM and Δ NOM (Figure 1d). By including both thermodynamic and dynamic ocean-atmosphere coupling, the SST in Δ NOM increases more uniformly in both hemispheres (Figure 1c). Isolating the effects of dynamic coupling, by subtracting the SST response in Δ SOM from Δ FOM, shows that ocean heat transport acts to transfer heat between the two hemispheres and thus to cool the NH and warm the SH (Figure 1e; Deser et al., 2016; Tomas et al., 2016).

The above temperature patterns are not confined to the surface but extend into the atmosphere as well (middle row in Figure 1). Without any ocean-atmosphere coupling, atmospheric warming in Δ NOM is confined to high latitudes in the NH (Figure 1f). Ocean thermodynamic coupling, however, deepens the NH high-latitude warming into the free troposphere, allowing the warming signal to reach into the upper tropical troposphere and into the SH (Figures 1g and 1i). Adding dynamic ocean-atmosphere coupling results in a more symmetric warming around the equator, which resembles the pattern under global warming (i.e., high-level tropical warming and surface-intensified Arctic warming; Figure 1h). Similar to the SST response, dynamic ocean-atmosphere coupling acts to cool the troposphere in the NH and warm it in the SH (Figure 1j; Deser et al., 2015, 2016).

In order to examine the response of the HC to Arctic sea ice melting, we start by showing the response of Ψ in the Δ NOM, Δ SOM, and Δ FOM configurations (colors in bottom row in Figure 1, where black contours show Ψ in the 20th century run). In Δ NOM, since the warming signal is confined to the pole, Arctic sea ice

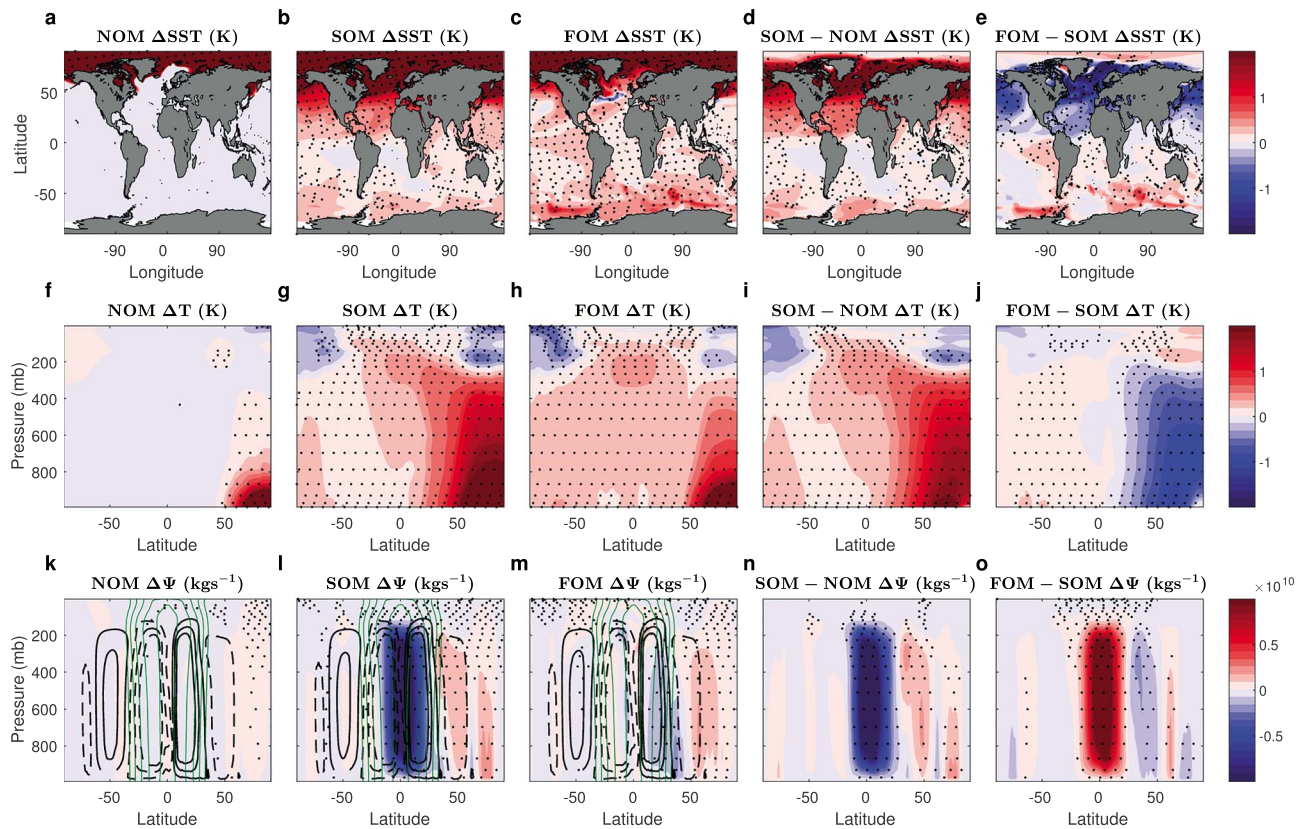


Figure 1. Response of the mean (a–e) SST (K), (f–j) zonal mean temperature (K), and (k–o) meridional mass stream function (kg/s) to late 21st century Arctic sea ice loss in the (first column) NOM, (second column) SOM, (third column) FOM, and the difference (fourth column) between SOM and NOM and (fifth column) between FOM and SOM. Black contours in panels k–m show the stream function at the end of the 20th century, with solid (dashed) contours representing clockwise (counterclockwise) circulation. Green contours in panels k–m show the mean angular momentum lines, with $0.2 \text{ m}^2/\text{s}$ spacing. The black dots indicate the regions where the response is statistically significant at the 95% confidence level. SST = sea surface temperature; NOM = no active ocean model; SOM = slab ocean model; FOM = full-depth ocean model.

loss has only a minor effect on the HC (Figure 1k). In ΔSOM , however, as in Tomas et al. (2016) and Wang et al. (2018), thermodynamic coupling weakens the NH HC (blue colors on solid contours in Figures 1l and 1n). The HC also weakens in ΔFOM (Figure 1m), but with a smaller magnitude than in ΔSOM , thus showing the effect of the dynamic coupling in strengthening the NH HC (Figure 1o), as reported under CO_2 doubling (Chemke & Polvani, 2018). To further examine the HC response to Arctic sea ice loss, we now analyze the responses of the three HC metrics.

3.1. The Northern Edge of the HC

Without any ocean coupling $\varphi_{\psi 500}$ in ΔNOM shows a minor shift of -0.16° , but with a large uncertainty ($\Delta\varphi_{\psi 500}$, yellow bar in Figure 2a). Adding thermodynamic coupling results in a clear northward shift of $\varphi_{\psi 500}$ of 0.85° in ΔSOM (blue bar). Dynamic coupling, however, overcomes this expansion and results in a southward shift of $\varphi_{\psi 500}$ of -0.32° in ΔFOM (red bar). Similar to the equatorward shift of the midlatitude jet and contraction of the ITCZ under Arctic sea ice loss (e.g., Deser et al., 2015, 2016; Screen et al., 2018), this southward shift opposes the projected northward shift of $\varphi_{\psi 500}$ under the RCP8.5 scenario (0.75° purple bar) by $\sim 40\%$. This further emphasizes the importance of ocean heat transport in carrying the Arctic signal to lower latitudes and in reducing the atmospheric thermodynamic response, as was also found under increased greenhouse gases (Chemke & Polvani, 2018).

Given the significant effect of Arctic sea ice loss on $\varphi_{\psi 500}$, we next seek to elucidate the mechanisms. Held (2000) developed a theory for the HC width, which is able to explain the projected widening of the HC (e.g., Chemke & Polvani, 2019). In that theory, the edge of the HC ($\varphi_{\text{H}00}$) is determined by the latitude where the vertical shear of the mean angular momentum conserving flow at the upper branch of the HC becomes baroclinically unstable and scales as follows:

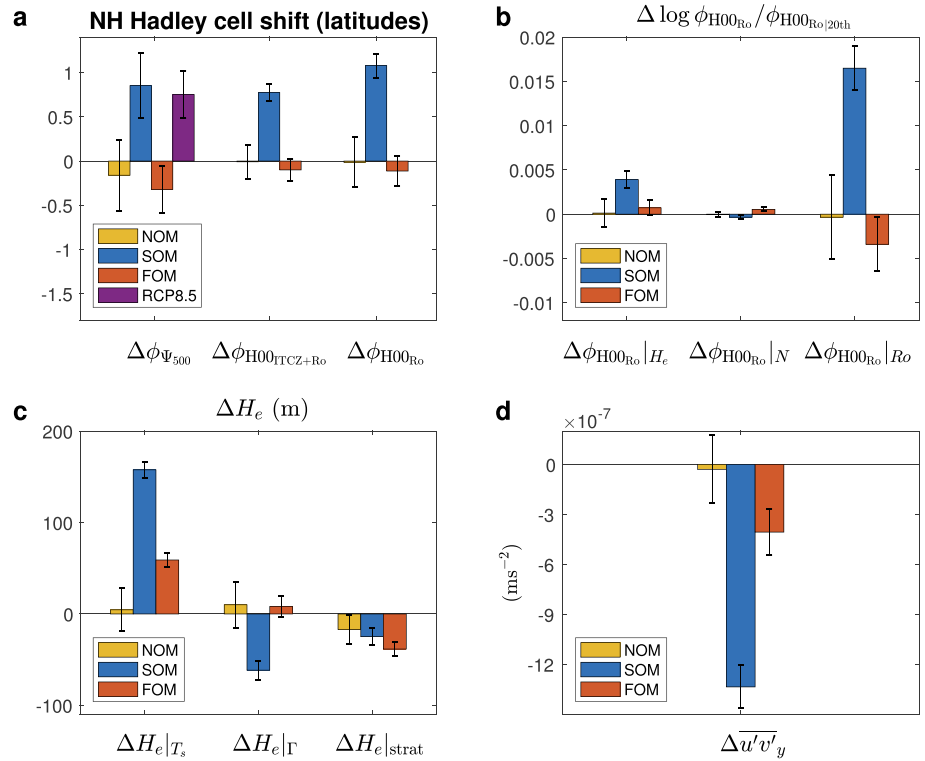


Figure 2. NH HC edge response to Arctic sea ice loss. (a) Latitudinal shift of the NH HC edge ($\Delta\phi_{\psi_{500}}$, section 2); and those predicted by the theory of Held (2000) with Ro and ITCZ taken from the simulations ($\Delta\phi_{H00ITCZ+Ro}$, equation (4)); and with only Ro taken from the simulations ($\Delta\phi_{H00Ro}$, equation (5)). (b) Relative contributions to the response of $\Delta\phi_{H00Ro}$: subtropical tropopause height ($\Delta\phi_{H00Ro}|_{H_e}$), static stability ($\Delta\phi_{H00Ro}|_N$), and tropical Rossby number ($\Delta\phi_{H00Ro}|_{Ro}$; equation (6)). (c) The relative contributions to the subtropical tropopause height response: subtropical surface temperature ($\Delta H_e|_{T_s}$), tropospheric lapse rate ($\Delta H_e|_{\Gamma}$), and stratospheric temperature and lapse rate ($H_e|_{strat}$). (d) The response of the tropical eddy momentum flux divergence. In all panels yellow, blue, and red bars show ΔNOM , ΔSOM , and ΔFOM , respectively, and the vertical error bars represent the 95% confidence interval. The purple bar in panel a shows the RCP8.5 response. NH = Northern Hemisphere; HC = Hadley cell; ITCZ = Intertropical Convergence Zone; RCP = Representative Concentration Pathway; NOM = no active ocean model; SOM = slab ocean model; FOM = full-depth ocean model.

$$\phi_{H00} \propto \left(\frac{NH_e}{\Omega a} \right)^{1/2}, \quad (2)$$

where H_e is subtropical tropopause height, $N^2 = \frac{g}{\theta} \frac{\partial \theta}{\partial z}$ is subtropical static stability (averaged between 400 and 800 mb), and Ω is Earth's rotation rate. The angular momentum flow, however, is affected by both the presence of eddies within the upper branch of the HC and the latitudinal position of the ITCZ (Kang & Lu, 2012). Given the effects of Arctic sea ice loss on both eddy momentum fluxes (e.g., Oudar et al., 2017; Sun et al., 2015) and ITCZ position (e.g., Deser et al., 2015; Smith et al., 2017; Tomas et al., 2016; Wang et al., 2018), we next incorporate these effects in equation (2), as was done in Kang and Lu (2012).

Regarding the location of the ITCZ, since an air parcel starts to acquire angular momentum as it propagates poleward of the equator, if the ITCZ is located further north of the equator, for example, it would act to push $\phi_{\psi_{500}}$ further poleward, as it allows the mean flow to move further poleward before becoming baroclinically unstable. In addition, eddy momentum fluxes act to extract momentum from the mean flow, and thus angular momentum is not entirely conserved within the HC. Neglecting friction and vertical advection, the steady state zonal mean momentum equation can be written as follows:

$$f(1 - Ro)\bar{v} = \frac{1}{a \cos^2 \phi} \frac{\partial \overline{u'v'}}{\partial \phi} \cos^2 \phi, \quad (3)$$

where f is the Coriolis parameter, $Ro \equiv -\bar{\zeta}/f$ is the local Rossby number, $\bar{\zeta} = -\frac{1}{a \cos \phi} \frac{\partial \bar{u} \cos \phi}{\partial \phi}$ is mean relative vorticity, u is zonal wind, and prime represents deviation from zonal and time mean. Since $f(1 - Ro) = \frac{-1}{a^2 \cos \phi} \frac{\partial \bar{m}}{\partial \phi}$, where \bar{m} is mean angular momentum ($\bar{m} \equiv [\bar{u} + \Omega a \cos \phi] a \cos \phi$), and $\bar{v} > 0$ in the upper branch of the HC, angular momentum is conserved (i.e., $\frac{1}{a^2 \cos \phi} \frac{\partial \bar{m}}{\partial \phi} = 0$) only if the eddies vanish in the HC (i.e., the right-hand side [RHS] of equation (3) is 0). However, due to the presence of eddies within the HC, the angular momentum is not entirely conserved, as can be seen by the fact that the stream function crosses mean angular momentum lines in the upper branch of the HC (green lines in Figures 1k–1m). Based on equation (3), Ro can be used to measure the importance of eddies in reducing the mean angular momentum (Adam & Harnik, 2013; Walker & Schneider, 2006). As Ro approaches unity, the flow approaches its angular momentum conserving solution, while as Ro approaches 0, eddies play an important role in reducing angular momentum. Following Kang and Lu (2012; see their equation 8), one can include the tropical Ro (averaged over the upper branch between 200 and 400 mb) in the Held (2000) theory, as well as a northward displacement of the ITCZ of the equator ($\varphi_{ITCZ} > 0$ for all NOM, SOM, and FOM simulations). Then, the HC width scaling can be written as follows:

$$\phi_{H00_{ITCZ+Ro}} \propto 0.25 \left\{ \phi_{ITCZ}^2 + \left(\phi_{ITCZ}^4 + \left[\frac{NH_e}{\Omega a Ro^{1/2}} \right]^2 \right)^{1/2} \right\}^{1/2}. \quad (4)$$

When $Ro = 1$ (i.e., when the flow conserves angular momentum) and $\varphi_{ITCZ} = 0$ (i.e., the ITCZ is on the equator), equation (4) reduces to equation (2). A decrease in Ro (i.e., strengthening of the eddies) pushes $\phi_{H00_{Ro}}$ poleward, since the eddies extract momentum from the mean flow, which allows the mean flow to move further poleward before becoming baroclinically unstable. Similar arguments can be applied for a northward shift of φ_{ITCZ} .

Equation (4) (with a constant of proportionality of 1) qualitatively captures both the northward shift of $\varphi_{\psi 500}$ in Δ SOM (blue bar, 0.78°) and the southward shift of $\varphi_{\psi 500}$ in Δ FOM (red bar, -0.1° ; $\Delta \phi_{H00_{ITCZ+Ro}}$; Figure 2a). To elucidate which components in $\phi_{H00_{ITCZ+Ro}}$ are responsible for these shifts in Δ SOM and Δ FOM, we first examine the importance of changes in φ_{ITCZ} . This is done by recalculating equation (4) while keeping $\varphi_{ITCZ} = 0$, which yields

$$\phi_{H00_{Ro}} \propto \left(\frac{NH_e}{\Omega a Ro^{1/2}} \right)^{1/2}. \quad (5)$$

Equation (5) gives results similar to equation (4) (compare $\Delta \phi_{H00_{Ro}}$ and $\Delta \phi_{H00_{ITCZ+Ro}}$ in Figure 2a), implying that ITCZ shifts have minor effects on the response of $\varphi_{\psi 500}$ under Arctic sea ice loss. In order to further examine which of the components in equation (5) is responsible for the HC edge changes, we take the logarithm of equation (5) after dividing it by its twentieth century value,

$$\log \left(\frac{\phi_{H00_{Ro}}}{\phi_{H00_{Ro_{20th}}}} \right) = 0.5 \log \left(\frac{N}{N_{20th}} \right) + 0.5 \log \left(\frac{H_e}{H_{e_{20th}}} \right) - 0.25 \log \left(\frac{Ro}{Ro_{20th}} \right). \quad (6)$$

The relative contributions of the RHS of equation (6) are shown in Figure 2b. Unlike the poleward shift of $\varphi_{\psi 500}$ under global warming that was found to occur due, primarily, to changes in subtropical static stability (Chemke & Polvani, 2019), here the northward shift of $\varphi_{\psi 500}$ in Δ SOM (blue bar) is linked to both an increase in H_e ($\Delta \phi_{H00_{Ro}}|_{H_e}$) and a decrease in Ro ($\Delta \phi_{H00_{Ro}}|_{Ro}$), whereas the southward shift of $\varphi_{\psi 500}$ in Δ FOM (red bar) is linked to an increase in Ro . This shows that unlike $\phi_{H00_{Ro}}$ (equation (5)), φ_{H00} (equation (2)) alone could not explain the shift of $\varphi_{\psi 500}$. These two variables (H_e and Ro) also show the largest difference between Δ SOM and Δ FOM and thus capture the different roles of thermodynamic and dynamic ocean-atmosphere coupling.

To gain further understanding on the physical processes that affect the response of H_e and Ro for both Δ SOM and Δ FOM, we further analyze each of these components. Changes in H_e can be due to both changes in the mean temperature and the temperature lapse rate (e.g., Thuburn & Craig, 2000; Vallis et al., 2015). Assuming constant tropospheric (Γ_{trop}) and stratospheric (Γ_{strat}) lapse rates, these changes can be isolated from the stratospheric temperature (T_{strat}) equation,

$$T_{strat}(z) = T_s + \Gamma_{trop} H_e + \Gamma_{strat} (z - H_e), \quad (7)$$

where T_s is surface temperature. Isolating H_e in the above equation leads to an equation for ΔH_e ,

$$\Delta H_e = -\frac{\Delta T_s}{\Gamma_{\text{trop}} - \Gamma_{\text{strat}}} - \frac{H_e \Delta \Gamma_{\text{trop}}}{\Gamma_{\text{trop}} - \Gamma_{\text{strat}}} + \frac{\Delta T_{\text{strat}} - \Delta \Gamma_{\text{strat}}(z - H)}{\Gamma_{\text{trop}} - \Gamma_{\text{strat}}}, \quad (8)$$

which is similar to equation 9 in Vallis et al. (2015) but here also accounts for changes in a nonisothermal stratosphere. The terms on the RHS in equation (8) account for changes in subtropical surface temperature, tropospheric lapse rate, and stratospheric temperature and lapse rate, respectively. The relative contributions of the different terms are plotted in Figure 2c. Changes in T_s ($\Delta H_e|_{T_s}$) are mostly responsible for the increase in H_e in ΔSOM (blue bar) and for the reduced increase in H_e in ΔFOM (red bar). Thus, the cooling of the NH due to ocean heat transport (Figure 1e) results in a weaker increase in H_e under Arctic sea ice loss, which leads to a weaker HC poleward expansion.

Since R_o is defined using the mean zonal flow ($-\bar{\zeta}/f$), any northward or equatorward shift of $\phi_{H00_{R_o}}$ due to changes in R_o may not be due to changes in eddies but might simply represent changes in the mean zonal flow itself. To examine whether changes in R_o stem from changes in eddy momentum fluxes, changes in the divergence of the tropical eddy momentum fluxes ($\Delta u'v'_y$), averaged over the upper branch the HC between 200 and 400 mb, are shown in Figure 2d. Confirming previous studies (e.g., Oudar et al., 2017; Sun et al., 2015), the eddies within the HC weaken in both ΔSOM (blue bar) and ΔFOM (red bar). A weakening of the eddies implies an increase in R_o and thus a southward shift of $\phi_{H00_{R_o}}$ (equation (5)). Hence, the decrease in R_o in ΔSOM simply represents the changes in the mean zonal flow (partly associated with the shift of the HC itself) and not the weakening of the eddies. That weakening, which acts to shift $\phi_{H00_{R_o}}$ southward, does not overcome the poleward shift of $\phi_{H00_{R_o}}$ in ΔSOM due to the increased H_e (as discussed above). In ΔFOM , however, the tendency of ocean heat transport to cool the surface, and thus to reduce the increase in H_e , allows the weakening of eddy momentum fluxes to push $\phi_{H00_{R_o}}$ southward.

3.2. The HC Strength

As was shown in Figures 1k–1o, the NH HC strength ($\Delta\Psi_{\text{max}}$) shows minor changes in ΔNOM ($-6.9 \cdot 10^6$ kg/s, yellow bar in Figure 3a), strong weakening in ΔSOM ($-6.7 \cdot 10^9$ kg/s, blue bar), and a small weakening in ΔFOM ($-0.91 \cdot 10^9$ kg/s, red bar). The latter, as also found under CO_2 doubling (Chemke & Polvani, 2018), reveals the opposite effects of the thermodynamic and dynamic ocean-atmosphere coupling, which weaken and strengthen the HC under Arctic sea ice loss, respectively (Tomas et al., 2016; Wang et al., 2018). Note, also, that the weakening in ΔFOM is a relatively small fraction ($\sim 12\%$) of the weakening of the HC under the RCP8.5 scenario ($-7.3 \cdot 10^9$ kg/s, purple bar).

To further analyze the weakening of the HC under Arctic sea ice loss, we investigate the stream function equation (the Kuo-Eliassen equation, Kuo, 1956), which is derived using quasi-geostrophic approximation and thermal wind balance (section 14.5.5 in Peixoto & Oort, 1992),

$$f^2 \frac{g}{2\pi a \cos \phi} \frac{\partial^2 \psi}{\partial p^2} + S^2 \frac{g}{2\pi a} \frac{1}{a} \frac{\partial}{\partial \phi} \frac{1}{\cos \phi} \frac{\partial \psi}{\partial \phi} = \frac{R}{p} \left(\frac{1}{a} \frac{\partial \overline{Q_{\text{diab}}}}{\partial \phi} - \frac{1}{a^2 \cos \phi} \frac{\partial^2 \overline{v'T'}}{\partial \phi^2} \cos \phi \right) + f \left(\frac{1}{a \cos^2 \phi} \frac{\partial^2 \overline{u'v'} \cos^2 \phi}{\partial p \partial \phi} - \frac{\partial \overline{X}}{\partial p} \right), \quad (9)$$

where $S^2 = -\frac{1}{\rho \theta} \frac{\partial \theta}{\partial p}$ is static stability in pressure coordinates, ρ is density, $R = 287 \text{ J} \cdot \text{kg}^{-1} \cdot \text{K}^{-1}$ is the gas constant of dry air, $\overline{Q_{\text{diab}}}$ is diabatic heating, $\overline{v'T'}$ is eddy heat fluxes, and \overline{X} is zonal friction. Several studies have suggested that $\overline{Q_{\text{diab}}}$ and S^2 are responsible for the weakening of the circulation in the future (e.g., Bony et al., 2013; Knutson & Manabe, 1995; Merlis, 2015). Here we solve equation (9), with the RHS specified from the model's output, using a successive overrelaxation method. The solution of equation (9) ($\Delta\Psi_{\text{max}_{\text{Eq}}}$) shows a similar response to Arctic sea ice loss as diagnosed from the model (Figure 3a): It captures the minor changes in ΔNOM , the strong weakening in ΔSOM , and the small weakening in ΔFOM .

To gain further understanding on the HC strength responses to Arctic sea ice loss under the different configurations of ocean-atmosphere coupling, equation (9) is solved separately for each term on the RHS. The contribution of each term in equation (9) along with that of the LHS operator (S^2 ; cf. equation 12 in Kim & Lee, 2001a; calculated at 500 mb at the latitude of Ψ_{max}) is plotted in Figure 3b. The weakening of the HC in ΔSOM (blue bars) is accompanied with changes in all components, but mainly with diabatic heating ($\Delta\Psi|_{Q_{\text{diab}}}$). In ΔFOM (red bars), similar to the HC width response, the reduction in eddy momentum

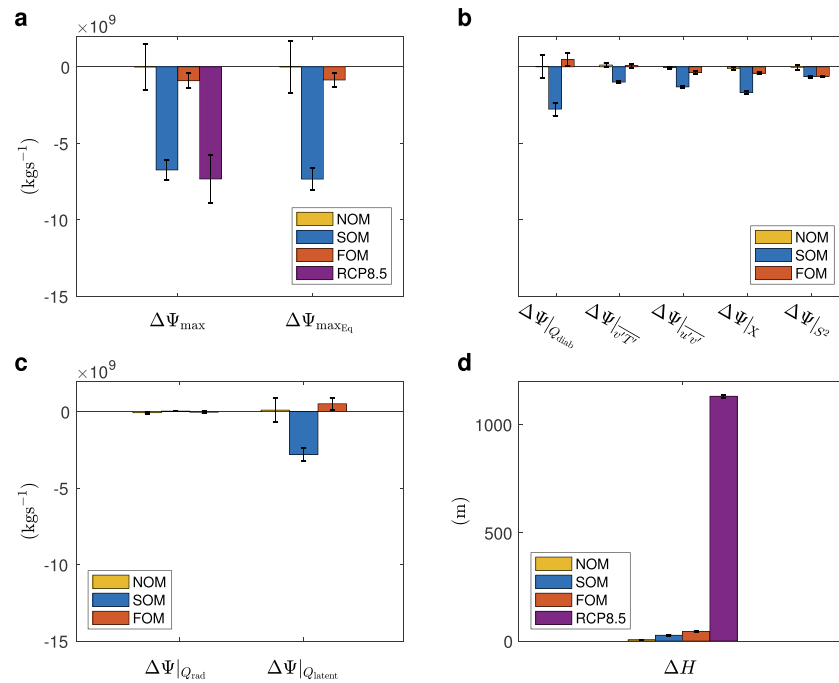


Figure 3. NH HC strength and height responses to Arctic sea ice loss. (a) The response of the NH HC strength (kg/s) computed from equation (1) ($\Delta\Psi_{\max}$) and the Kuo-Eliassen equation (equation (9); $\Delta\Psi_{\max Eq}$). (b) The relative contribution of the different terms in equation (9) (kg/s): diabatic heating ($\Delta\Psi|_{Q_{diab}}$), eddy heat fluxes ($\Delta\Psi|_{v'T'}$), eddy momentum flux ($\Delta\Psi|_{u'v'}$), zonal friction ($\Delta\Psi|_{\chi}$), and static stability ($\Delta\Psi|_{s^2}$). (c) The contribution of the diabatic heating term in equation (9) separated into contributions from radiative heating ($\Delta\Psi|_{Q_{rad}}$) and latent heating ($\Delta\Psi|_{Q_{latent}}$). (d) The tropical tropopause height response to Arctic sea ice loss (ΔH , m; section 2). In all panels, yellow, blue, and red bars show Δ NOM, Δ SOM, and Δ FOM, respectively, and the vertical error bars represent the 95% confidence interval. The purple bar in panels a and d show the RCP8.5 response. NH = Northern Hemisphere; HC = Hadley cell; NOM = no active ocean model; SOM = slab ocean model; FOM = full-depth ocean model. RCP = Representative Concentration Pathway.

fluxes ($\Delta\Psi|_{u'v'}$) together with zonal friction ($\Delta\Psi|_{\chi}$) and static stability ($\Delta\Psi|_{s^2}$) contribute to the weakening of the circulation. The diabatic heating also accounts for the largest difference between Δ SOM and Δ FOM responses (although the eddy fluxes also contribute to this discrepancy). Further decomposing the diabatic heating to contributions from radiative ($\Delta\Psi|_{Q_{rad}}$) and latent heating ($\Delta\Psi|_{Q_{latent}}$) shows that most of the difference between Δ SOM and Δ FOM comes from latent heating (Figure 3c). Similar to the response of the HC strength under CO_2 doubling (Chemke & Polvani, 2018), the cooling of the NH by ocean heat transport (Figure 1j) reduces the amount of water vapor available for condensation, which reduces the amount of latent heating, and thus acts to reduce the weakening of the HC under Arctic sea ice loss. Note that at steady state the RHS terms are not independent from each other (e.g., Kim & Lee, 2001b). Hence, this effect of latent heating may not necessarily be a direct response to Arctic sea ice loss but may stem from changes in the other terms in equation (9).

3.3. The HC Height

Unlike the above two metrics, Arctic sea ice loss has a very minor effect on the height (H) of the HC in Δ NOM (5.6 m, yellow bar in Figure 3d), Δ SOM (36.5 m, blue bar), and Δ FOM (44.7 m, red bar). In comparison, H increases by 1.1 km under the RCP8.5 scenario (purple bar in Figure 3d).

4. Conclusions

We have here examined the impact of future Arctic sea ice melting on the annual mean NH HC. Our findings add to the large literature which has focused on the response of midlatitude circulation and the ITCZ to Arctic sea ice loss (e.g., Barnes & Polvani, 2015; Barnes & Screen, 2015; Deser et al., 2015, 2016; Oudar et al., 2017; Peings & Magnusdottir, 2014; Screen et al., 2018; Sun et al., 2015; Smith et al., 2017; Tomas et al., 2016; Wang et al., 2018). Given the importance of ocean-atmosphere coupling in carrying the Arctic signal to

lower latitudes, we used a hierarchy of model configurations (atmosphere only, slab ocean, and fully coupled ocean-atmosphere) to simulate the Arctic sea ice state at the end of the 20th and 21st centuries.

We have found that the strength and poleward edge of the NH HC respond to Arctic sea ice loss only when accounting for ocean-atmosphere coupling. In response to Arctic sea ice loss, the warming of the NH due to thermodynamic ocean-atmosphere coupling increases the tropopause height, resulting in a northward shift of the NH HC edge. The NH warming also increases the latent heating and decreases eddy momentum fluxes, which together weaken the NH HC.

Dynamic ocean-atmosphere coupling, however, acts to cool the NH, which reduces latent heating, and cancels most of the NH HC weakening. The cooling induced by ocean heat transport changes also reduces the increase in tropopause height, which together with the weakening of the eddy momentum fluxes overcomes the thermodynamic northward expansion and acts to contract the NH HC. This contraction opposes the overall projected widening in response to RCP8.5 radiative forcing by $\sim 40\%$. Hence, the melting of Arctic sea ice acts as a *negative internal feedback* in the response of the tropical circulation to increased greenhouse gases. This adds to the findings of previous studies and provides one more instance of Arctic sea ice loss causing the atmospheric circulation to oppose its projected response, mostly through changes in ocean heat transport (e.g., Deser et al., 2015, 2016).

Our findings also confirm the results of previous studies which investigated the effects of high-latitude forcing on the HC. In particular, previous studies showed that in both slab and full-depth ocean models warming (cooling) the surface in NH high latitudes, in comparison to SH high latitudes, also results in a weakening (strengthening) of the HC (e.g., Chiang & Bitz, 2005; Green & Marshall, 2017; Kang et al., 2009). More importantly, as previously reported, the effects of Arctic sea ice loss at lower latitudes occur through ocean-atmosphere coupling (e.g., Chiang & Bitz, 2005; Deser et al., 2015, 2016; Green & Marshall, 2017; Tomas et al., 2016; Wang et al., 2018): This highlights the importance of accounting for this coupling when assessing the response of the climate system to anthropogenic forcing (e.g., Armour et al., 2016; Chemke & Polvani, 2018; Deser et al., 2016; Lu & Zhao, 2012; Singh et al., 2017; Winton, 2003).

Ocean-atmosphere coupling not only affects the annual mean response of the HC but its seasonality as well. The seasonality of the HC response is similar to the annual mean response, since sea ice loss occurs across all seasons (Deser et al., 2015). The magnitude of the response, however, does vary across seasons due to the seasonal cycle of sea ice and the response time of ocean-atmosphere coupling. In future work we plan to examine the effect of Antarctic sea ice loss on the HC, which was also found to result in atmospheric circulation changes that oppose their response to increased greenhouse gases (England et al., 2018).

Acknowledgments

We thank Bob Tomas and Lantao Sun for providing the data of the simulations. R. C. is supported by the NOAA Climate and Global Change Postdoctoral Fellowship Program, administered by UCAR's Cooperative Programs for the Advancement of Earth System Science (CPAESS). LMP is funded by a grant from the National Science Foundation to Columbia University. NCAR is sponsored by the National Science Foundation.

References

- Adam, O., & Harnik, N. (2013). Idealized annually averaged macroturbulent Hadley circulation in a shallow-water model. *Journal of the Atmospheric Sciences*, *70*, 284–302.
- Armour, K. C., Marshall, J., Scott, J. R., Donohoe, A., & Newsom, E. R. (2016). Southern Ocean warming delayed by circumpolar upwelling and equatorward transport. *Nature Geoscience*, *9*, 549–554.
- Barnes, E. A. (2013). Revisiting the evidence linking Arctic amplification to extreme weather in midlatitudes. *Geophysical Research Letters*, *40*, 4734–4739. <https://doi.org/10.1002/grl.50880>
- Barnes, E. A., & Polvani, L. M. (2015). CMIP5 projections of Arctic amplification, of the North American/North Atlantic circulation, and of their relationship. *Journal of Climate*, *28*, 5254–5271.
- Barnes, E. A., & Screen, J. A. (2015). The impact of Arctic warming on the midlatitude jet-stream: Can it? Has it? Will it? *Wiley Interdisciplinary Reviews: Climate Change*, *6*(3), 277–286.
- Blackport, R., & Kushner, P. J. (2016). The transient and equilibrium climate response to rapid summertime sea ice loss in CCSM4. *Journal of Climate*, *29*, 401–417.
- Bony, S., Bellon, G., Klocke, D., Sherwood, S., Fermepin, S., & Denvil, S. (2013). Robust direct effect of carbon dioxide on tropical circulation and regional precipitation. *Nature Geoscience*, *6*, 447–451.
- Chemke, R., & Polvani, L. M. (2018). Ocean circulation reduces the Hadley cell response to increased greenhouse gases. *Geophysical Research Letters*, *45*, 9197–9205. <https://doi.org/10.1029/2018GL079070>
- Chemke, R., & Polvani, L. M. (2019). Exploiting the abrupt 4xCO₂ scenario to elucidate tropical expansion mechanisms. *Journal of Climate*, *32*(3), 859–875. <https://doi.org/10.1175/JCLI-D-18-0330.1>
- Chiang, J. C. H., & Bitz, C. M. (2005). Influence of high latitude ice cover on the marine intertropical convergence zone. *Climate Dynamics*, *25*, 477–496.
- Cohen, J., Screen, J. A., Furtado, J. C., Barlow, M., Whittleston, D., Coumou, D., et al. (2014). Recent Arctic amplification and extreme mid-latitude weather. *Nature Geoscience*, *7*, 627–637.
- Deser, C., Sun, L., Tomas, R. A., & Screen, J. (2016). Does ocean coupling matter for the northern extratropical response to projected Arctic sea ice loss? *Geophysical Research Letters*, *43*, 2149–2157. <https://doi.org/10.1002/2016GL067792>

- Deser, C., Tomas, R. A., & Sun, L. (2015). The role of ocean-atmosphere coupling in the zonal-mean atmospheric response to Arctic sea ice loss. *Journal of Climate*, *28*, 2168–2186.
- England, M., Polvani, L. M., & Sun, L. (2018). Contrasting the Antarctic and Arctic atmospheric responses to projected sea ice loss in the late twenty-first century. *Journal of Climate*, *31*(16), 6353–6370.
- Gent, P. R., Danabasoglu, G., Donner, L. J., Holland, M. M., Hunke, E. C., Jayne, S. R., et al. (2011). The community climate system model version 4. *Journal of Climate*, *24*, 4973–4991.
- Green, B., & Marshall, J. (2017). Coupling of trade winds with ocean circulation damps ITCZ shifts. *Journal of Climate*, *30*, 4395–4411.
- Hassanzadeh, P., & Kuang, Z. (2015). Blocking variability: Arctic amplification versus Arctic oscillation. *Geophysical Research Letters*, *42*, 8586–8595. <https://doi.org/10.1002/2015GL065923>
- Held, I. M. (2000). The general circulation of the atmosphere. Program in geophysical fluid dynamics. Woods Hole, MA: Woods Hole Oceanographic Institute. Retrieved from <https://www.whoi.edu>
- Held, I. M., & Soden, B. J. (2006). Robust responses of the hydrological cycle to global warming. *Journal of Climate*, *19*, 5686–5699.
- Intergovernmental Panel on Climate Change (2013). Summary of policymakers. In T. F. Stocker (Ed.), *Climate change 2013: The physical basis* (pp. 1–29). Cambridge: Cambridge University Press.
- Kang, S. M., Deser, C., & Polvani, L. M. (2013). Uncertainty in climate change projections of the Hadley circulation: The role of internal variability. *Journal of Climate*, *26*, 7541–7554.
- Kang, S. M., Frierson, D. M. W., & Held, I. M. (2009). The tropical response to extratropical thermal forcing in an idealized GCM: The importance of radiative feedbacks and convective parameterization. *Journal of the Atmospheric Sciences*, *66*, 2812.
- Kang, S. M., Held, I. M., Frierson, D. M. W., & Zhao, M. (2008). The response of the ITCZ to extratropical thermal forcing: Idealized slab-ocean experiments with a GCM. *Journal of Climate*, *21*, 3521.
- Kang, S. M., & Lu, J. (2012). Expansion of the Hadley cell under global warming: Winter versus summer. *Journal of Climate*, *25*, 8387–8393.
- Kim, H.-K., & Lee, S. (2001a). Hadley cell dynamics in a primitive equation model. Part I: Axisymmetric flow. *Journal of the Atmospheric Sciences*, *58*(19), 2845–2858.
- Kim, H.-K., & Lee, S. (2001b). Hadley cell dynamics in a primitive equation model. Part II: Nonaxisymmetric flow. *Journal of the Atmospheric Sciences*, *58*, 2859–2871.
- Knutson, T. R., & Manabe, S. (1995). Time-mean response over the tropical pacific to increased CO₂ in a coupled ocean-atmosphere model. *Journal of Climate*, *8*, 2181–2199.
- Kuo, H.-L. (1956). Forced and free meridional circulations in the atmosphere. *Journal of the Atmospheric Sciences*, *13*, 561–568.
- Lu, J., Vecchi, G. A., & Reichler, T. (2007). Expansion of the Hadley cell under global warming. *Geophysical Research Letters*, *34*, L06805. <https://doi.org/10.1029/2006GL028443>
- Lu, J., & Zhao, B. (2012). The role of oceanic feedback in the climate response to doubling CO₂. *Journal of Climate*, *25*, 7544–7563.
- Merlis, T. M. (2015). Direct weakening of tropical circulations from masked CO₂ radiative forcing. *Proceedings of the National Academy of Sciences of the United States of America*, *112*(43), 13,167–13,171.
- Oudar, T., Sanchez-Gomez, E., Chauvin, F., Cattiaux, J., Terray, L., & Cassou, C. (2017). Respective roles of direct GHG radiative forcing and induced Arctic sea ice loss on the Northern Hemisphere atmospheric circulation. *Climate Dynamics*, *49*, 3693–3713.
- Overland, J., Francis, J. A., Hall, R., Hanna, E., Kim, S.-J., & Vihma, T. (2015). The melting Arctic and midlatitude weather patterns: Are they connected? *Journal of Climate*, *28*, 7917–7932.
- Peings, Y., & Magnusdottir, G. (2014). Response of the wintertime Northern Hemisphere atmospheric circulation to current and projected Arctic sea ice decline: A numerical study with CAM5. *Journal of Climate*, *27*, 244–264.
- Peixoto, J. P., & Oort, A. H. (1992). *Physics of climate*. New York: American Institute of Physics.
- S'evelllec, F., Fedorov, A. V., & Liu, W. (2017). Arctic sea-ice decline weakens the Atlantic meridional overturning circulation. *Nature Climate Change*, *7*, 604–610.
- Screen, J. A., Deser, C., Smith, D. M., Zhang, X., Blackport, R., Kushner, P. J., et al. (2018). Consistency and discrepancy in the atmospheric response to Arctic sea-ice loss across climate models. *Nature Geoscience*, *11*, 155–163.
- Screen, J. A., Deser, C., & Sun, L. (2015). Reduced risk of North American cold extremes due to continued Arctic sea ice loss. *Bulletin of the American Meteorological Society*, *96*, 1489–1503.
- Screen, J. A., & Simmonds, I. (2013). Exploring links between Arctic amplification and mid-latitude weather. *Geophysical Research Letters*, *40*, 959–964. <https://doi.org/10.1002/GRL.50174>
- Singh, H. A., Rasch, P. J., & Rose, B. E. J. (2017). Increased ocean heat convergence into the high latitudes with CO₂ doubling enhances polar-amplified warming. *Geophysical Research Letters*, *44*, 10. <https://doi.org/10.1002/2017GL074561>
- Smith, D. M., Dunstone, N. J., Scaife, A. A., Fiedler, E. K., Copsey, D., & Hardiman, S. C. (2017). Atmospheric response to Arctic and Antarctic sea ice: The importance of ocean-atmosphere coupling and the background state. *Journal of Climate*, *30*, 4547–4565.
- Sun, L., Deser, C., & Tomas, R. A. (2015). Mechanisms of stratospheric and tropospheric circulation response to projected Arctic sea ice loss*. *Journal of Climate*, *28*, 7824–7845.
- Sun, L., Perlwitz, J., & Hoerling, M. (2016). What caused the recent “warm Arctic, cold continents” trend pattern in winter temperatures? *Geophysical Research Letters*, *43*, 5345–5352. <https://doi.org/10.1002/2016GL069024>
- Thuburn, J., & Craig, G. C. (2000). Stratospheric influence on tropopause height: The radiative constraint. *Journal of the Atmospheric Sciences*, *57*, 17–28.
- Tomas, R. A., Deser, C., & Sun, L. (2016). The role of ocean heat transport in the global climate response to projected Arctic sea ice loss. *Journal of Climate*, *29*, 6841–6859.
- Vallis, G. K., Zurita-Gotor, P., Cairns, C., & Kidston, J. (2015). Response of the large-scale structure of the atmosphere to global warming. *Quarterly Journal of the Royal Meteorological Society*, *141*, 1479–1501.
- Vihma, T. (2014). Effects of Arctic sea ice decline on weather and climate: A review. *Surveys in Geophysics*, *35*, 1175–1214.
- Walker, C. C., & Schneider, T. (2006). Eddy influences on Hadley circulations: Simulations with an idealized GCM. *Journal of the Atmospheric Sciences*, *63*, 3333–3350.
- Walsh, J. E. (2014). Intensified warming of the Arctic: Causes and impacts on middle latitudes. *Global and Planetary Change*, *117*, 52–63.
- Wang, K., Deser, C., Sun, L., & Tomas, R. A. (2018). Fast response of the tropics to an abrupt loss of Arctic sea ice via ocean dynamics. *Geophysical Research Letters*, *45*, 4264–4272. <https://doi.org/10.1029/2018GL077325>
- Winton, M. (2003). On the climatic impact of ocean circulation. *Journal of Climate*, *16*, 2875–2889.
- Zhang, R., & Delworth, T. L. (2005). Simulated tropical response to a substantial weakening of the Atlantic thermohaline circulation. *Journal of Climate*, *18*, 1853–1860.